Biomimetic approach for an articular cartilage patch: combination of decellularized cartilage matrix and silk-elastin-like-protein (SELP) hydrogel

Annals of Anatomy

Biomimetic approach for an articular cartilage patch: combination of decellularized cartilage matrix and silk-elastin-like-protein (SELP) hydrogel

--Manuscript Draft--

Manuscript Number:	AANAT5290R1
Article Type:	VSI: New veterinary anatomy - Original Article
Keywords:	Articular Cartilage; Decellularized Extracellular Matrix; Silk-Elastin-Like Protein; Chondrocytes
Corresponding Author:	Matteo Zoboli ITALY
First Author:	F. Ravanetti
Order of Authors:	F. Ravanetti
	P. Borghetti
	M. Zoboli
	P. M. Veloso
	E. De Angelis
	R. Ciccimarra
	R. Saleri
	A. Cacchioli
	F. Gazza
	R. Machado
	L. Ragionieri
	C. Attanasio
Abstract:	Articular cartilage degradation due to injury, disease and aging is a common clinical issue as current regenerative therapies are unable to fully replicate the complex microenvironment of the native tissue which, being avascular, is featured by very low ability to self-regenerate. The extracellular matrix (ECM), constituting almost 90% of the entire tissue, plays a critical role in its function and resistance to compressive forces. In this context, the current tissue engineering strategies are only partially effective in restoring the biology and function of the native tissue. A main issue in tissue regeneration is treatment failure due to scarce integration of the engineered construct, often following a gradual detachment of the graft. In this scenario, we aimed to create an adhesive patch able to adequately support cartilage regeneration as a promising tool for the treatment of cartilage injuries and diseases. For this, we produced an engineered construct composed of decellularized ECM (dECM) obtained from horse joint cartilage, to support tissue regeneration, coupled with a Silk-Elastin-Like Proteins (SELP) hydrogel, which acts as a biological glue, to guarantee an adequate adherence to the host tissue. Following the production of the two biomaterials we characterized them by assessing: 1) dECM morphological, chemical, and ultrastructural features along with its capability to support chondrocyte proliferation, specific marker expression and ECM synthesis; 2) SELP microarchitecture, cytocompatibility and mechanical properties. Our results, demonstrated that both materials hold unique properties suitable to be exploited to produce a tailored microenvironment to support cell growth and differentiation providing a proof of concept concerning the in vitro biological and mechanical efficacy of the construct. The SELP hydrogel displayed a very interesting physical behavior due to its high degree of resistance to mechanical stress, which is generally associated with physiological mechanical load during locomotion. Intriguingly, the shear-thinning behavior of the hydrogel may also make it suitable to be applied and spread over non-homogeneous surfaces, therefore, we hypothesize that the hybrid biomaterial

	proposed may be a real asset in the treatment of cartilage defects and injuries.
Suggested Reviewers:	Sivia Clotilde Bianca Modina, Prof University of Milan Faculty of Veterinary Medicine silvia.modina@unimi.it
	Marco Patruno Prof marco.pat@unipd.it

Figure 1

Click here to access/download;Figure;Fig1.JPG

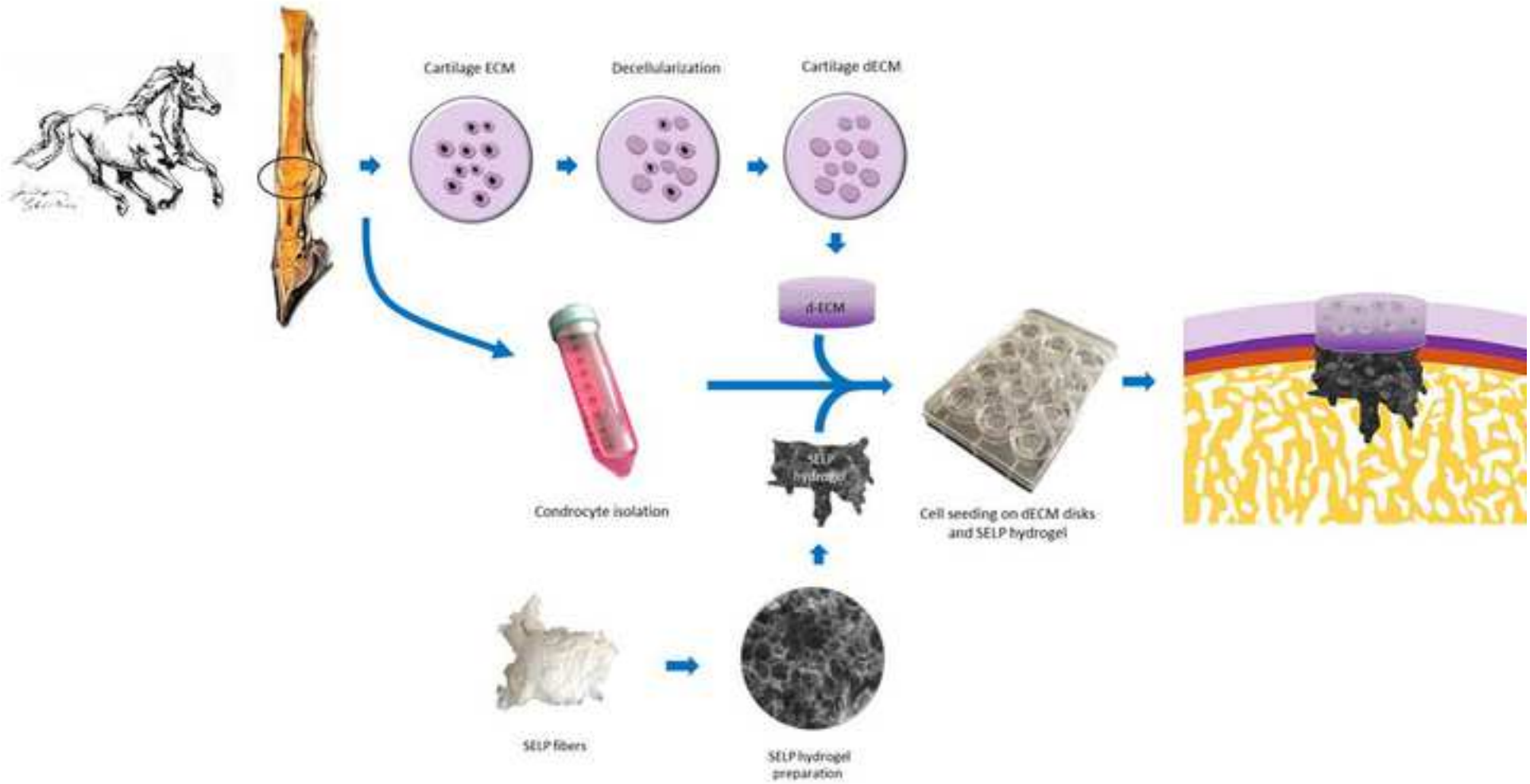

Figure 2

Click here to access/download;Figure;Fig2.jpg

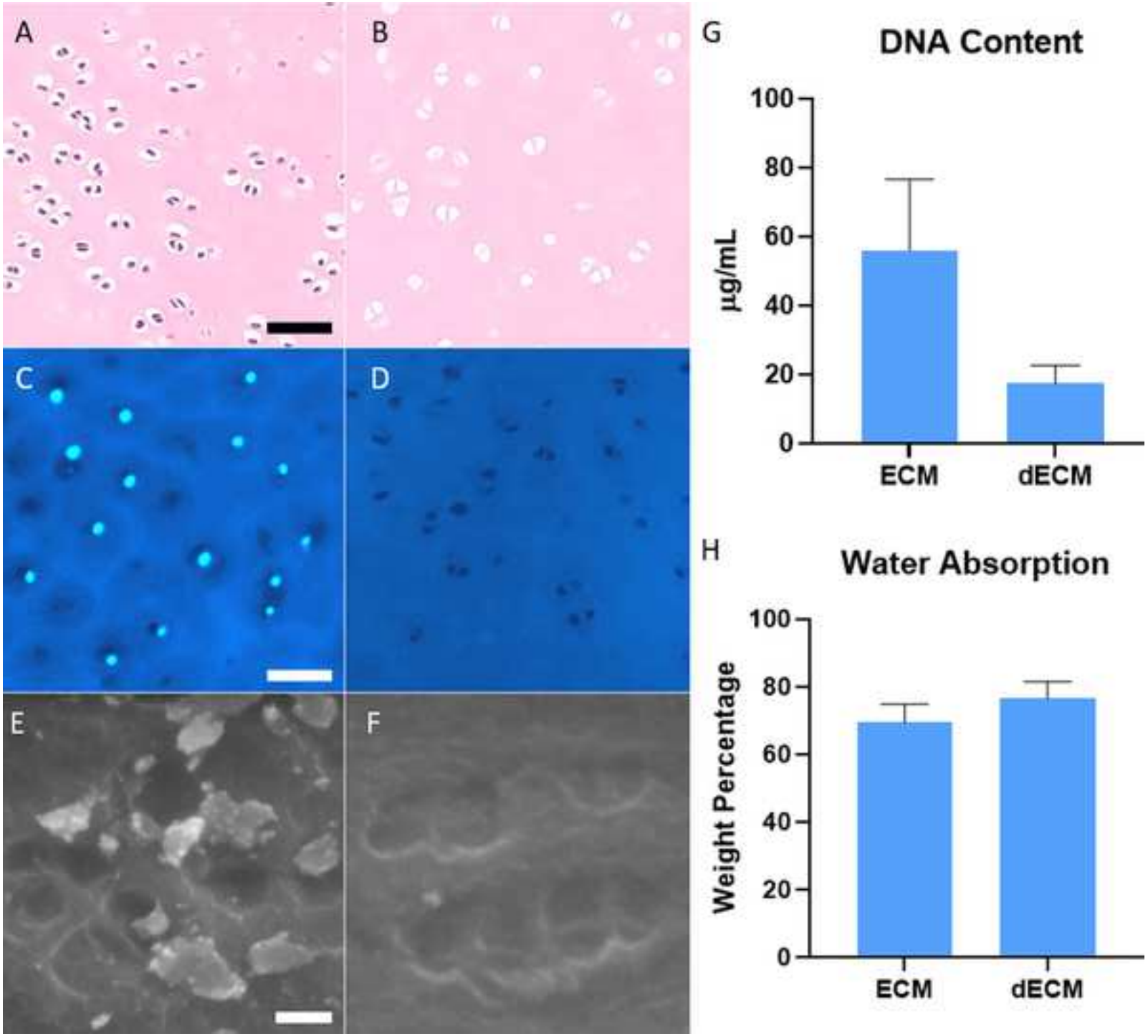

Figure 3

Click here to access/download;Figure;Fig3.jpg

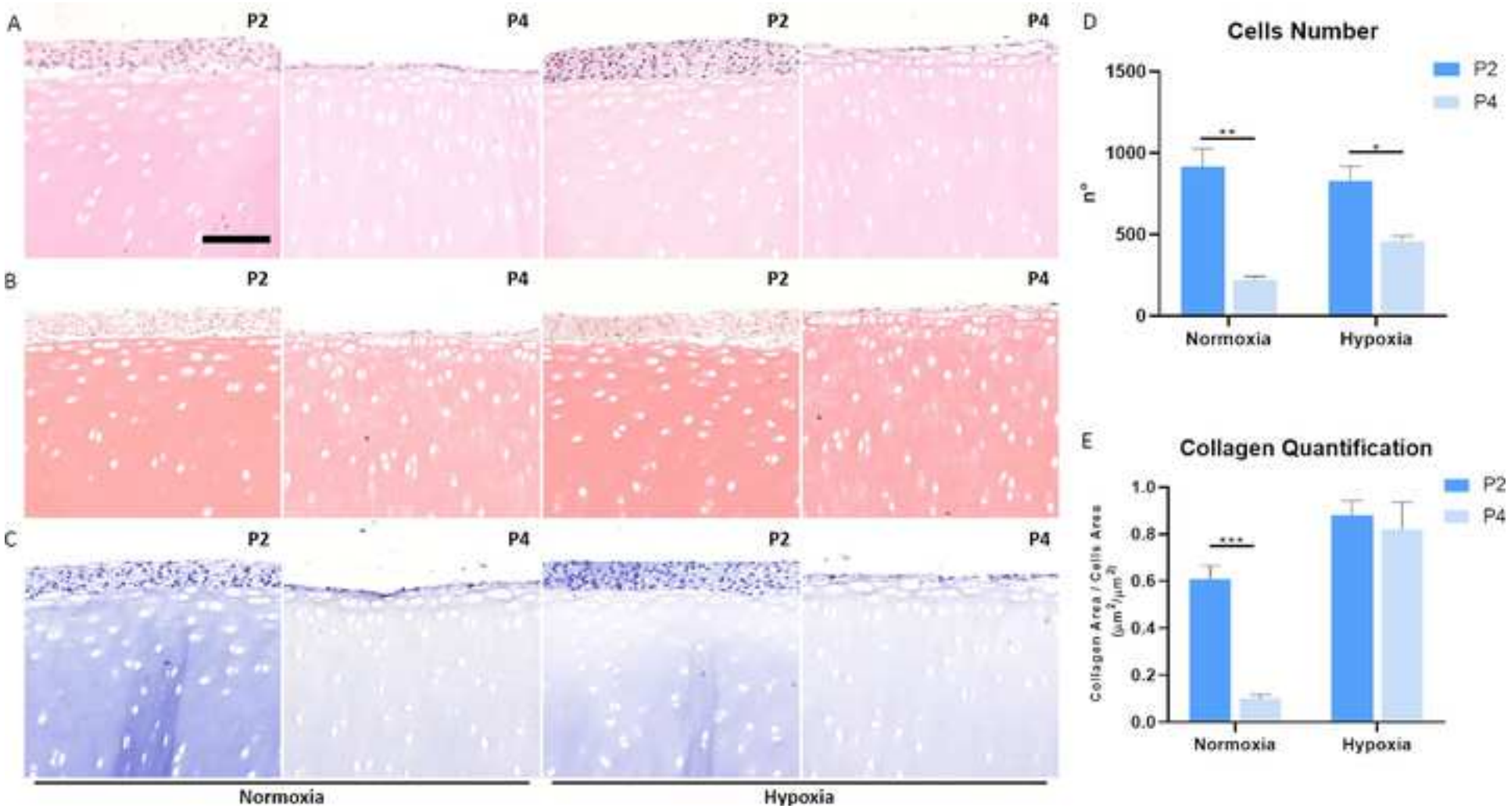

Figure 4

Click here to access/download;Figure;Fig4.jpg

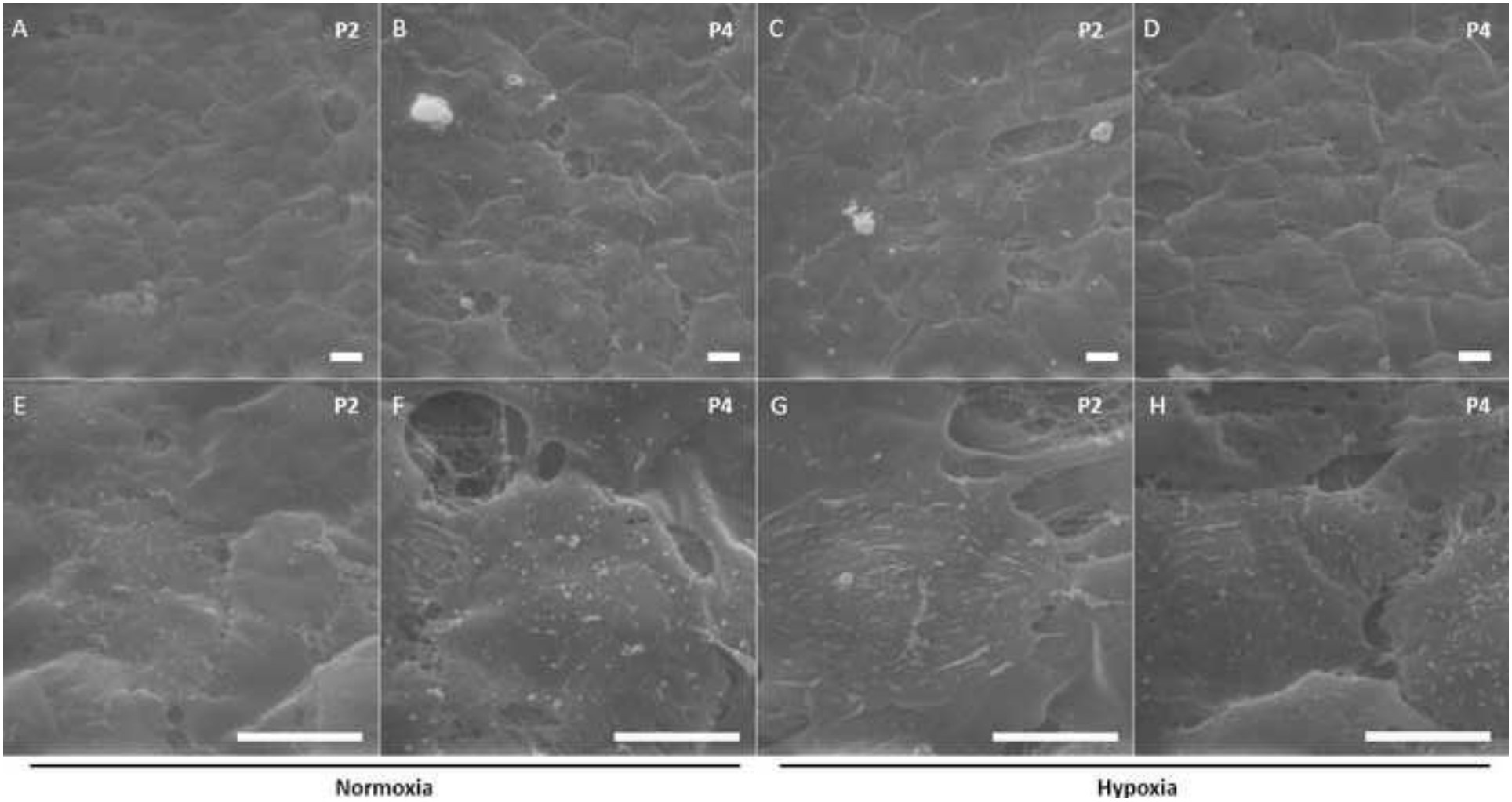

Figure 5

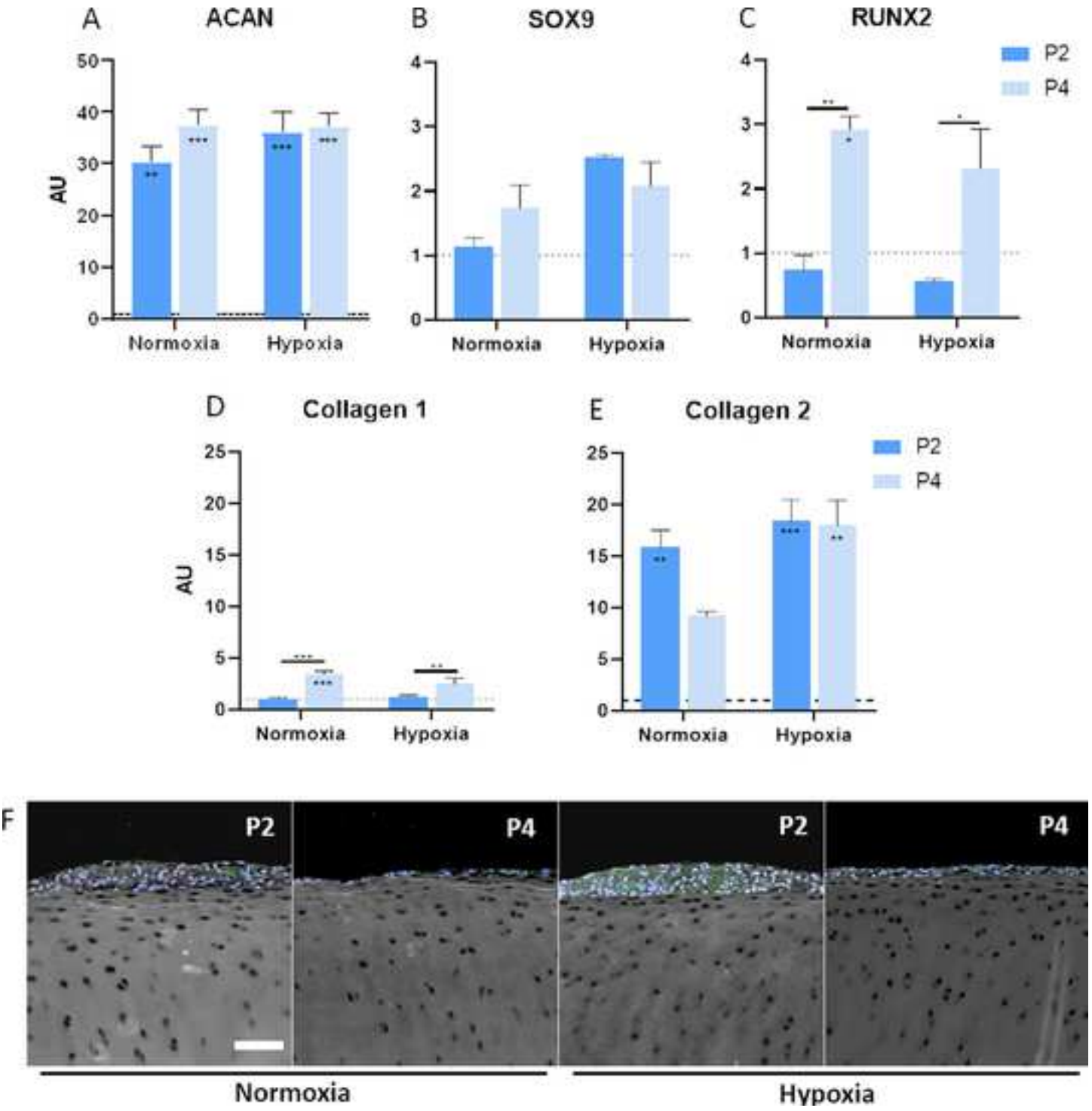

Figure 6

Click here to access/download;Figure;Fig6.jpg

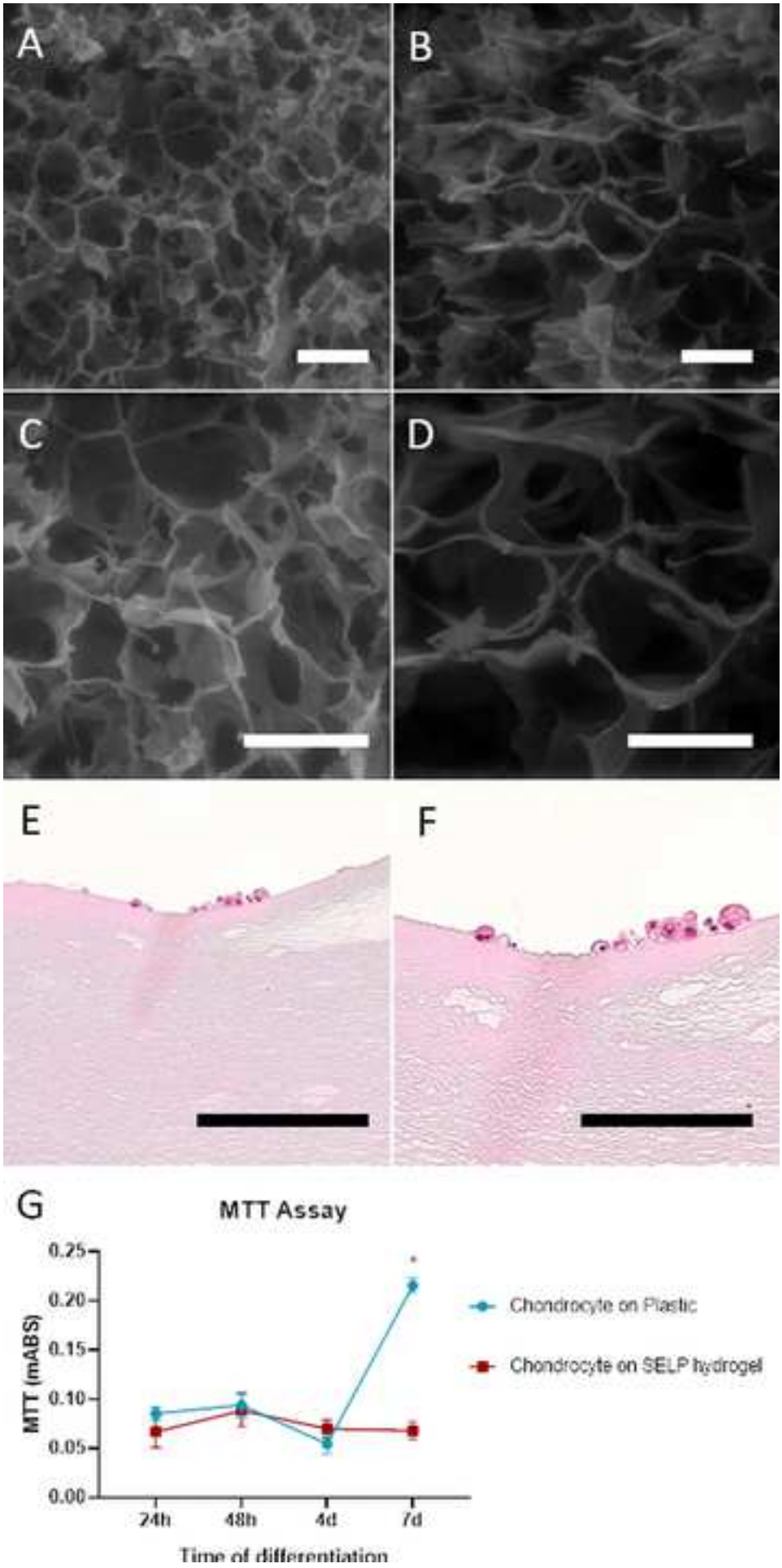

Figure 7

Click here to access/download;Figure;Fig7.jpg

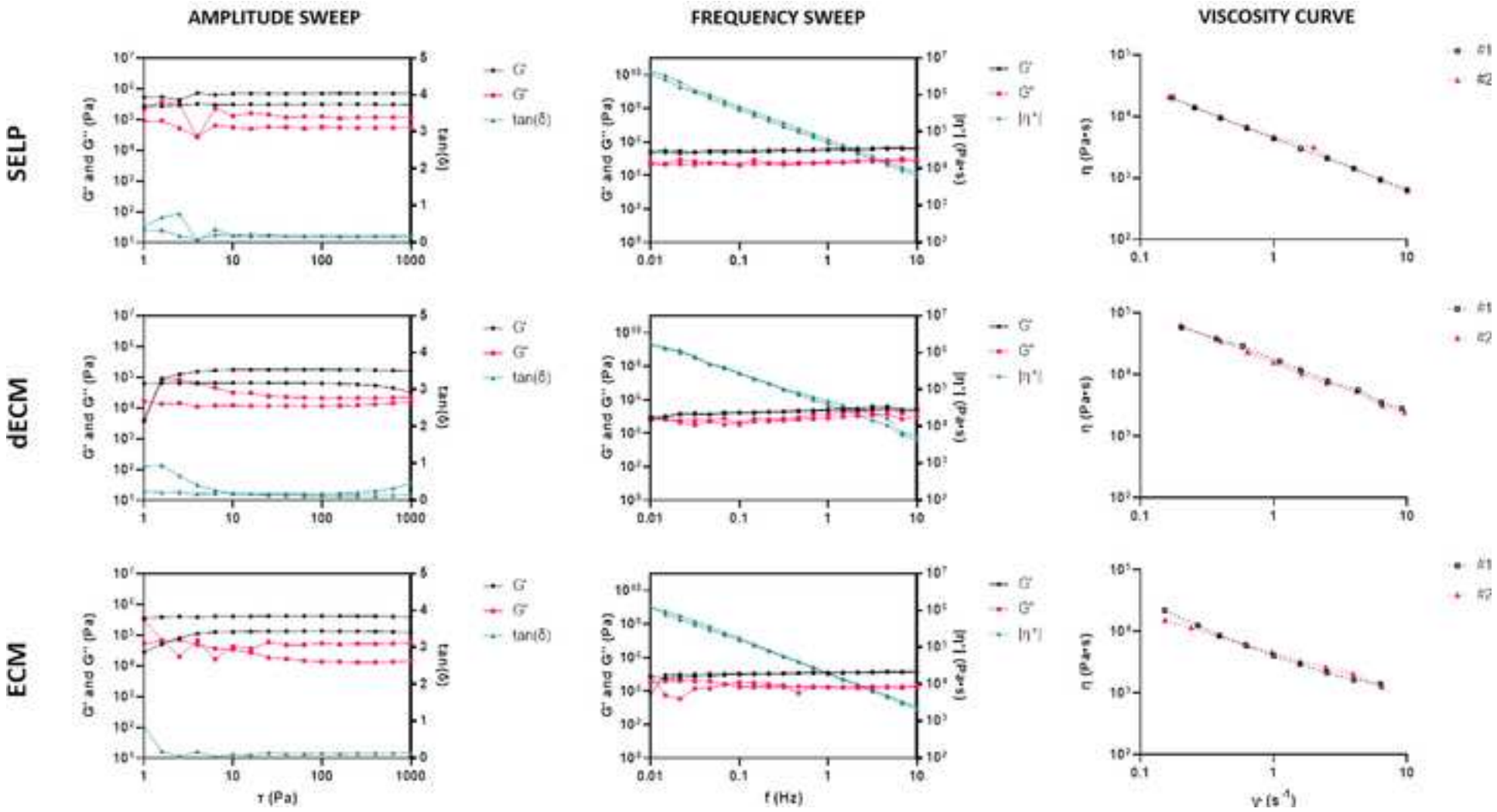

Figure 8

A

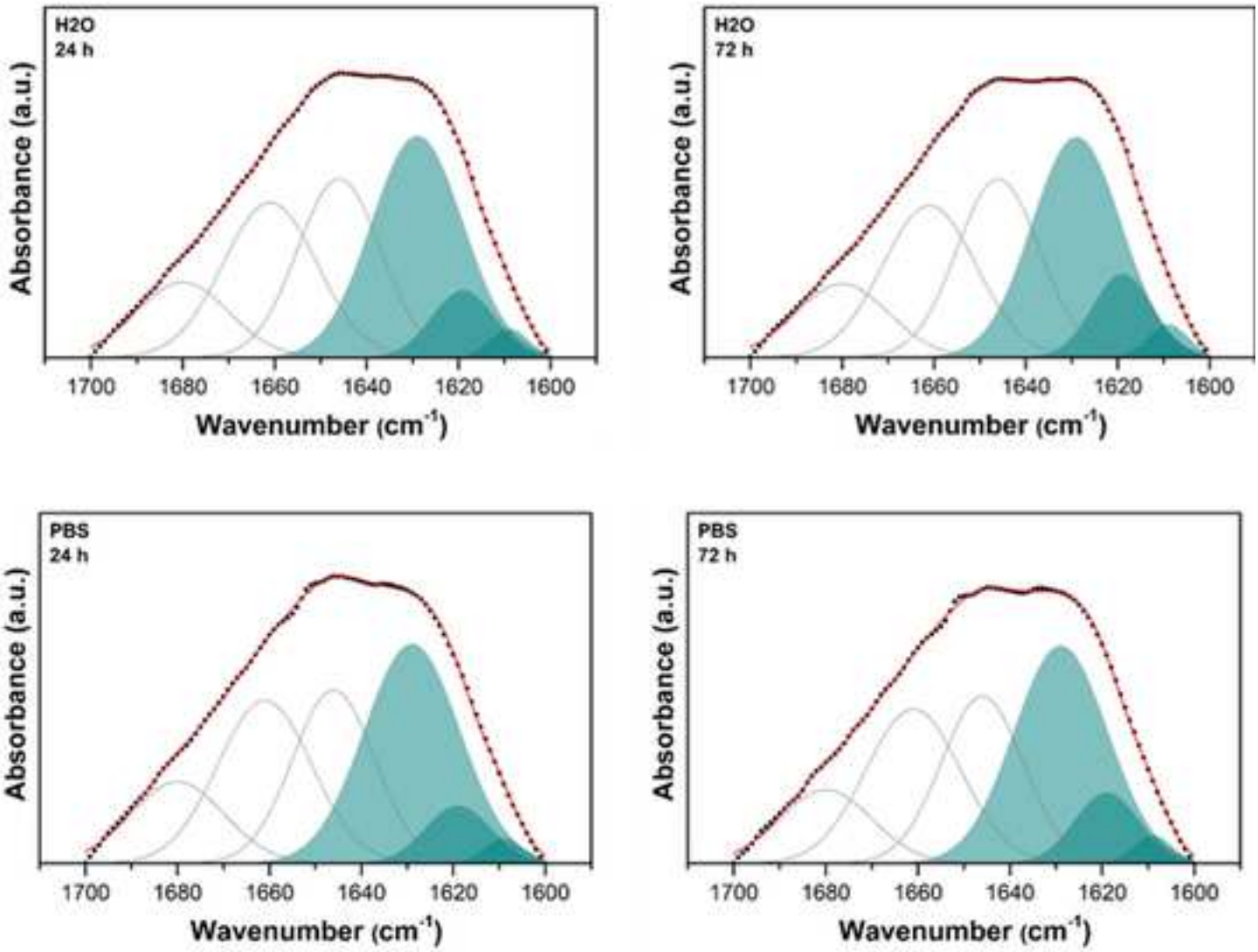

B

Fractional distribution of secondary structures

	β- structures	random coils	turns and bends
H_2O 24 h	52.3	24.0	23.7
H_2O 72 h	52.8	24.0	23.2
PBS 24 h	52.7	22.8	24.5
PBS 72 h	53.4	22.6	24.1

Biomimetic approach for an articular cartilage patch: combination of decellularized cartilage matrix and silk-elastin-like-protein (SELP) hydrogel

F. Ravanetti[1], P. Borghetti[1], M. Zoboli[1]*, P. M. Veloso[1,+], E. De Angelis[1], R. Ciccimarra[1], R. Saleri[1], A. Cacchioli[1], F. Gazza[1], R. Machado[2], L. Ragionieri[1]°, C. Attanasio °[3]

[1] Department of Veterinary Science, University of Parma

[2] Centre of Molecular and Environmental Biology (CBMA), Department of Biology and Institute of Science and Innovation for Bio-Sustainability (IB-S), University of Minho, Braga, Portugal

[3] Department of Veterinary Medicine and Animal Production, University of Naples Federico II

[+]present address: Department of Biomedical Sciences, University of Padua

° the two authors contributed equally to this work

*** Corresponding author**

Abstract

Articular cartilage degradation due to injury, disease and aging is a common clinical issue as current regenerative therapies are unable to fully replicate the complex microenvironment of the native tissue which, being avascular, is featured by very low ability to self-regenerate. The extracellular matrix (ECM), constituting almost 90% of the entire tissue, plays a critical role in its function and resistance to compressive forces. In this context, the current tissue engineering strategies are only partially effective in restoring the biology and function of the native tissue. A main issue in tissue regeneration is treatment failure due to scarce integration of the engineered construct, often following a gradual detachment of the graft. In this scenario, we aimed to create an adhesive patch able to adequately support cartilage regeneration as a promising tool for the treatment of cartilage injuries and diseases. For this, we produced an engineered construct composed of decellularized ECM (dECM) obtained from horse joint cartilage, to support tissue regeneration, coupled with a Silk-Elastin-Like Proteins (SELP) hydrogel, which acts as a biological glue, to guarantee an adequate adherence to the host tissue. Following the production of the two biomaterials we characterized them by assessing: 1) dECM morphological, chemical, and ultrastructural features along with its capability to support chondrocyte proliferation, specific marker expression and ECM synthesis; 2) SELP microarchitecture, cytocompatibility and mechanical properties. Our results, demonstrated that both materials hold unique properties suitable to be exploited to produce a tailored microenvironment to support cell growth and differentiation providing a proof of concept concerning the in vitro biological and mechanical efficacy of the construct. The SELP hydrogel displayed a very interesting physical behavior due to its high degree of resistance to mechanical stress, which is generally associated with physiological mechanical load during locomotion. Intriguingly, the shear-thinning behavior of the hydrogel may also make it suitable to be applied and spread over non-homogeneous surfaces, therefore, we hypothesize that the hybrid biomaterial proposed may be a real asset in the treatment of cartilage defects and injuries.

Keywords: Articular Cartilage; Decellularized Extracellular Matrix; Silk-Elastin-Like Protein; Chondrocytes

1 Introduction

Articular cartilage damage and degeneration caused by injury, disease and aging are very common clinical issues. Regenerative therapies are currently unable to replicate the specific microenvironment of the native articular cartilage (Jiang et al., 2021; Nurul et al., 2021; Xie et al., 2021). This highly hydrated, avascular tissue displays complex morphological and chemical features, mainly related to the microarchitecture of its extracellular matrix (ECM), which makes up around 90% of the total volume of the tissue. Articular cartilage (AC) is divided into four compartments holding a differential microarchitecture comprising a superficial zone, a transitional zone, a deep zone and a calcified zone. Each of them contributes differently to mechanical loading, highlighting the critical role of this zonal arrangement for tissue function, particularly for its resistance to compressive forces, making it essential for the protection of the underlying subchondral bone. Cartilage is a hypocellular, avascular, aneural, and alymphatic tissue, resulting in limited self-repair capacity after injuries (Karuppal, 2017). In particular, the lack of vascularization limits the infiltration of progenitor cells and the consequent ability of the tissue to self-regenerate. Cell‐based therapies have demonstrated a disease‐modifying effect on osteoarthritis in preclinical animal models, representing a favorable therapeutic approach (Boffa et al., 2023). However, lost cartilage is often replaced by fibrocartilage that is mechanically inferior compared to native tissue (Armiento et al., 2019).

Cartilage tissue engineering includes several approaches attempting to address this open challenge through the use of synthetic materials (Stampoultzis et al., 2021). Although these latter can be modified to mimic the mechanical and biochemical properties of the cellular microenvironment, they generally fail to fully reproduce the multitude of interactions occurring in the native tissue. Most likely, this is due to the dynamic nature of some specific proteins composing the extracellular matrix, which probably underpins a more nuanced role for ECM in homeostasis and disease (Bonnans et al., 2014). Because of this complexity, research on cartilage regeneration has not yet reached satisfactory results thus making cartilage repair an open challenge in the clinical arena (Ngadimin et al., 2021).The decellularized ECM is currently considered a promising natural substrate for cartilage regeneration (Xia et al., 2019). The use of decellularization technology preserves natural tissue ECM, while simultaneously eliminating specific homogenous/xenogeneic cells in tissues or organs, allowing to synthesize minimally immunogenic scaffolds with key biological and biomechanical properties (Brown et al., 2022; Kasravi et al., 2023; Morris et al., 2017). To date, decellularized extracellular matrix (dECM) is a well-recognized biomaterial developed to engineer more than 15 types of tissues and organs, being able to preserve the native environment by promoting cell proliferation and providing biochemical cues for cell differentiation (Brown et al., 2022). Also, in materials science and tissue engineering, there is currently a widespread use of natural hydrogels, namely hydrophilic polymers networks able to absorb large amounts of water while maintaining their structure suitable to be used in different forms such as films, scaffolds, nanoparticles and drug carriers (Li et al., 2019; Wei et al., 2021; Zhang and Khademhosseini, 2017). In tissue regeneration approaches, to avoid treatment failure due to the detachment of components and to promote construct integration with the host tissue during regeneration, it is mandatory that the biomaterials adhere perfectly to the latter (Sani et al., 2019; Wang et al., 2007; Zhou et al., 2018). In this scenario, our approach aims to combine the use of dECM and a Silk-Elastin-Like Protein (SELP) hydrogel for the creation of a cartilage patch with suitable biological and mechanical properties, in which the SELP hydrogel acts as a powerful bioadhesive glue able to firmly bond the construct to the damaged cartilage area and to effectively guarantee its integration with the host tissue. SELPs are genetically engineered protein polymers that combine in the same polypeptide chain the properties of both silk and elastin (Machado et al., 2015, 2013b). Due to their versatility of processing and biocompatibility, SELPs have been engineered for a wide variety of biomedical applications (Correia et al., 2019; Machado et al., 2015; Shen et al., 2022; Varanko et al., 2020)**.** SELP-based therapies for cartilage regeneration are still in the very

early stages of development (Cipriani et al., 2018; Haider et al., 2008) but they are certainly very promising and with the advancement of research in this field, these recombinant protein polymers will likely become an increasingly important tool in the treatment of cartilage injuries and diseases.

2 Materials and methods

The experimental setup is summarized in Figure 1.

2.1 Articular Cartilage harvest

Articular cartilage was obtained from metacarpophalangeal and metatarsophalangeal joints of horses (*Equus ferus caballus*) ranging from 5 to 8 years old (n=8), slaughtered for human consumption in a slaughterhouse certified by the Italian Ministry of Health according to the Regulation (EC) 853/2004 (Zerbini & Ragazzi S.R.L., Correggio (RE), Italy; approval nr. CE-IT 798-M). Joints were immediately delivered to our laboratory and then used to collect the cartilage. After arthrotomy and cartilage exposure, the joints were carefully examined, and those with macroscopic lesions related to overt osteoarthritis (OA) or with evidence of synovitis were excluded from the study. Cartilage slices approximately 1 - 1.5 mm thick were cut with a surgical blade; to obtain standardized disks of cartilage, a punch of 8 mm (n = 192) diameter was used. Cartilage disks were immediately frozen in liquid nitrogen and stored at -80 °C until use. All the procedures were undertaken in a sterile environment.

2.2 Cartilage Decellularization

Frozen cartilage disks were defrosted at room temperature and incubated for 1 h at 37 °C, under gentle agitation, in a solution of 0.25% Trypsin + EDTA 1X. After two washing steps (5 min each) in Phosphate Buffered Saline (PBS), cartilage disks were incubated in 3 % Triton X-100/PBS, under agitation at 4 °C for 48 h. Subsequently, disks were rinsed twice in PBS (30 min each) and then incubated in 1 % Sodium Dodecyl Sulfate (SDS) at 4 °C under constant stirring for 24 h. After four washing cycles (20 min each), disks were incubated overnight (O/N) at 37 °C in a solution containing 1.5 mg/mL DNase and RNase in 0.15 M NaCl and 30 mM $MgCl_2 6H_2O$. Cartilage disks were soaked in a cartilage washing solution of PBS, 1% Pen-Strep and 1% amphotericin for 1 h and then treated with liquid nitrogen and stored at -80 °C. Before use, disks were sterilized by UV under a laminar flow hood (Thermo Scientific) for 30 min per each side, at 18–21 °C.

2.3 DNA content evaluation

The effectiveness of cartilage decellularization process was assessed through both nuclear counterstaining with DAPI (4',6-diamidino-2-phenylindole) and DNA content assay. For nuclear counterstaining, after deparaffinization and rehydration, sections were covered with 300 nM DAPI (Invitrogen) staining solution for 5 min and rinsed three times in PBS (5 min each). Fluorescent whole slide imaging (WSI) was acquired using a NanoZoomer S60 scanner (Hamamatsu Photonics K.K., Hamamatsu City, Japan) and DAPI fluorescence was detected. DNA content was evaluated by DNeasy quantification kit (Qiagen) following the manufacturer's instructions. DNA concentration (n=3) was measured at 260 nm using a nanodrop spectrophotometer (Thermo Scientific NanoDrop Lite Spectrophotometer).

2.4 Water absorption capacity

The initial dry weights of native equine and decellularized cartilage disks were carefully measured (W0). The scaffolds were then immersed in PBS at 37 °C (pH 7.4) for 8 h. Cartilage disks were taken out from PBS and the wet weights were recorded as W1. The water absorption ratio was determined by applying the following formula: $(W1 - W0)/W0 \times 100\%)$, where W0 and W1 are the initial and final weights of the scaffolds, respectively.

2.5 SELP preparation

The recombinant SELP was biologically produced in microbial cell factories and purified according to previously described procedures (Machado et al., 2013a). The complete amino acid sequence was previously reported and comprises 9 tandem repeats of 5 silk blocks (sequence GAGAGS) fused with 9 elastin blocks (sequence VPAVG) (Fernandes et al., 2018; Machado et al., 2013a). To prepare the SELP hydrogel, 32 mg of pure lyophilized SELP were weighed and then clipped and frayed using tweezers, to facilitate the subsequent solubilization in cold deionized water (dH_2O) or PBS (1X) for a concentration of 8% (v/v). Dissolution was ensured by maintaining the protein solution overnight at 4 °C under constant stirring (200 rpm). After dissolving, the gel-like solution was incubated for 24 h and 72 h in an oven at 37 °C and used for subsequent assays.

2.6 Rheological characterization

The viscoelastic properties of both dECM and SELP were measured using three types of rheological tests carried out using a rotational HAAKE Mars 60 (Thermo Scientific) measuring system with a gap of 0.5 mm between plates and described below.

- Amplitude sweep: tests were performed by applying a stress with increasing amplitudes, ranging from 1 to 1000 Pa, and a constant frequency of 1 Hz, to determine the linear viscoelastic range (LVER) (range where the elastic and viscous moduli are independent from the strain).
- Frequency sweep tests: the measurements were performed by applying a stress with increasing frequencies, ranging from 0.01 to 10 Hz at a constant oscillation amplitude of 50 Pa (within the linear viscoelastic range) to obtain the elastic and viscous moduli (G' and G'', respectively) along with the complex viscosity (η*).
- Viscosity curve: the measurement was performed by applying a shear rate increasing from 0.1 to 10 s^{-1} and calculating the respective viscosity.

All the tests were performed in duplicate at 37 °C to simulate the potential behavior of the biomaterials when in the body.

2.7 Structural characterization of SELP by ATR-FTIR

The secondary structure of the SELP-based materials was assessed by attenuated total reflection Fourier-transform infrared (ATR-FTIR) spectroscopy in a range between 4000 – 400 cm^{-1} using a Spectrum Two™ from Perkin Elmer (Perkin Elmer, Waltham, MA, USA) equipped with a diamond ATR. Spectra were collected with a resolution of 4 cm^{-1}. Analysis of the secondary structure content was carried out in the amide I band region (1700 – 1600 cm^{-1}) following the procedures described elsewhere (Correia et al., 2019; Pereira et al., 2021, 2017). Afterwards, the amide I band region was truncated and normalized, followed by baseline correction, using OriginPro 9.0 software (Or, Northampton, MA). Briefly, for component analysis, the second derivative spectra of amide I band were smoothed with an eleven-point Savitsky-Golay smoothing function. The number of components and their peak positions were determined by second derivatization and used as initial parameters for iteratively fitting with a Gaussian function ($R2 > 0.999$). To ensure a comparable secondary structure assignment across all the samples, curve fitting was performed using the same set of parameters. The structural conformations were assigned by reference to literature (Table 1) and the contribution of each fitted component to the amide I band was determined by integrating the area under the curve and normalizing the value for the total area of amide I.

Table 1. Vibrational band assignments used for the analysis of the secondary structure content (Machado et al., 2015; Pereira et al., 2021, 2017).

Wavenumber [cm^{-1}]	Secondary structure assignment
1605 – 1615	aggregated strands
1616 – 1621	aggregated beta-strand/beta-sheets (weak)1
1622 – 1627	beta-sheets (strong)[1]
1628 – 1637	beta-sheets (strong)[2]
1638 – 1655	random coils
1656 – 1662	alpha-helices
1663 – 1696	turns and bends
1697 – 1703	beta-sheets (weak)[1]

[1]Intermolecular beta-sheets [2]Intramolecular beta-sheets

2.8 Scanning Electron Microscopy

Scanning Electron Microscopy (SEM) was performed for SELP and for cartilage disks before and after decellularization to evaluate disk microstructure, and then, after cell seeding, to evaluate cell adhesion and interaction with the biomaterial. Samples were fixed with 2.5% glutaraldehyde in 0.1 M sodium cacodylate buffer (pH 7.3) for 2 h at 4 °C. After dehydration through a graded series of ethanol, specimens were critical-point dried with liquid carbon dioxide (CPD 030 Baltec, Wallruf, Germany) and then sputter-coated (Balzers device) with gold-palladium (Plano, Germany) with a SCD 040 coating device (Balzer Union, Wallruf, Germany). All the samples were observed using a Zeiss DSM 950 scanning electron microscope with accelerating voltage set at 10 KV (Zeiss, Jena, Germany).

2.9 Cell isolation and culture

Chondrocytes were isolated from the articular cartilage following a protocol previously described (De Angelis et al., 2020). Freshly isolated chondrocytes were plated (P1: passage 1; 2×10^4 cells/cm^2) in triplicate in a Petri dish (57 cm^2) (Sarstedt, Nümbrecht, Germany), cultured in DMEM with 4.5 g/L glucose (SIGMA Aldrich) and 10% FBS at 37 °C and 5% CO_2 in a humified atmosphere. Medium was replaced every three days until monolayer formation when chondrocytes were detached by 0.25% trypsin – 0.02% EDTA (SIGMA Aldrich) and counted using a Bürker hemocytometer. Then, 2×10^4 cells were seeded in a subsequent subculture (Passage P2, P3, P4). In the present study, isolated chondrocytes at both Passage number 2 (P2) and Passage number 4 (P4) (n= 3 each in triplicate) were used. A suspension of 2×10^4 cells/cm^2 cells were seeded in 6-well plates (Sarstedt, Nümbrecht, Germany) with and without the dECM disks and gelled SELP support, and then cultured in medium DMEM 4.5 g/L glucose supplemented with 50 µg/mL 2-phospho-L-ascorbic acid, with 10% FBS, and changed twice a week. Cells were incubated at 37 °C in normoxic (19% of O_2) or hypoxic (5% of O_2) conditions for the time specified for each single experiment.

2.10 Histology

Samples were fixed in 10% formalin for 24 h at 4 °C and histologically processed (Leica, HistoCore PEARLS). Sections of 5 µm were obtained with a rotary microtome (Slee Cut 6062; Slee Medical, Mainz, Germany) and stained with Hematoxylin and Eosin (H&E), Picro-Sirius Red Stain Kit (PSR), and Toluidine Blue stain kit (TB), following the manufacturer's instructions (Histo-Line Laboratories). The sections were acquired as whole slide images (WSI) by a digital slide scanner (Nanozoomer S-60, Hamamatsu, Japan).

2.11 Cells and Collagen Fiber Quantification

After two weeks of culture, the number of chondrocytes on decellularized cartilage was assessed using QuPath version 0.4.3 (Bankhead et al., 2017). For all samples, cells were detected at the interface between chondrocytes and cartilage in H&E stain, using the native tool of the software 'Cell Detection'. The connective component was evaluated on PSR stains using the 'Pixel Classifier' classification algorithm, trained on representative images, in 10 regions of interest (ROI) per sample. The area occupied by the connective component was compared to that of the ROI and expressed as a percentage of occupied area.

2.12 Cell viability

MTT assay was performed to evaluate chondrocytes viability on the SELP hydrogel. Chondrocytes were seeded in 24-well plates with a density of 1×10^4 cells/well cultured in DMEM and incubated with 20 µL (5 mg/mL) of MTT solution. After 4 h of incubation, the medium and the MTT solution were removed and cells were lysed with 150 µL DMSO. The precipitated formazan crystals were solubilized, and detection was performed at 490 nm using a Victor-3™ 1420 Multilabel Counter (PerkinElmer, Waltham, MA, USA).

2.13 Gene Expression analysis

Total RNA was extracted from cells seeded on plastic and on dECM using TRIreagent (Ambion, Inc., Austin, TX), according to the manufacturer's instructions. dECM disks were transferred into liquid nitrogen and disrupted with mortar and pestle. TRIreagent (1 ml) was then added to the powder and RNA was extracted according to the manufacturer's instructions. Purity and concentration were assessed by UV spectrophotometry (GeneQuant Pro, Amersham Pharmacia Biotech-GE Healthcare Life Sciences, Little Chalfont, UK) at 260/280 nm and 260/230 nm respectively. RNA integrity and quality was evaluated by using an Agilent Bioanalyzer 2100 and RNA 6000 Labchip kit (Agilent Technologies, Santa Clara, CA, USA).

Prior to cDNA synthesis, RNA samples were treated with DNAse (Sigma). Total RNA (1 µg/20 µL) was reverse-transcripted using a High-capacity cDNA Reverse Transcription kit (Applied Biosystems, Foster City, CA). The reverse-transcription reaction was performed according to the manufacturer's instructions, under the following thermal conditions: 10 min at 25 °C, 120 min at 37 °C followed by 5 min at 85 °C. cDNA samples were stored at 20 °C until PCR was performed.

cDNA concentration was assessed by UV-spectrophotometry (GeneQuant Pro) and 5 ng of each sample were used as a template for real-time quantitative PCR (qPCR) performed by using a StepOne thermocycler (Applied Biosystems, StepOne software v. 2.1). The cDNA (5 ng/20 µL) was amplified with Fast SYBR Green Master Mix (Applied Biosystems) along with specific sets of primers at 300 or 500 nM. The primers were designed based on published gene sequences or by using Primer Express® software package (Applied Biosystems) to create oligonucleotides with similar melting temperatures and minimal self-complementary, purchased from Eurofins MWG Operon (Ebersberg, Germany). Details of each primer set for detection of gene expression are reported in Table 2. The reference gene HPRT1 was selected as endogenous control according to minimal intra-/inter-assay variation. Samples were kept at 95 °C for 20 s (hold step) and then subjected to 40 cycles consisting of a denaturation step at 95 °C for 3 s followed by an annealing/extension step at 60 °C for 30 s. Fluorescence due to SYBR Green I incorporation was acquired at the end of the extension step. A no-RT and a no-template control (NTC) were included in each experiment. A melting curve analysis for specific amplification control was performed (from 60 °C to 95 °C) at the end of the amplification cycles. NTC controls were assumed as negative and reliable if the quantification cycle (Cq) was ≥35. Data were analyzed according to the 2-ΔΔCt method (Schmittgen and Livak, 2008) in which expression levels of each gene are normalized to the HPRT1 cDNA amount and expressed as arbitrary Unit (AU). All experiments were performed in triplicate.

Table 2. Sequences of primer pairs used for RT-qPCR analysis.

Gene/Protein designation	Forward (F) and reverse (R) primers	Concentration (nM)
HPRT1/Hypoxanthine phosphoribosyltransferase	F 5'-AATTATGGACAGGACTGAACGG-3' R 5'-ATAATCCAGCAGGTCAGCAAAG-3'	300
RUNX2	F 5'-CTGTGGTTACTGTCATGGCG-3' R 5'-TCGTTGAACCTTGCCACTTG-3'	300
COL1A1/Collagen type I alpha 1 chain	F 5'-AGAAGAAGACATCCCAGCAGTCA-3' R 5'-CAGGGCTCGGGTTTCCATA-3'	500
COL2A1/Collagen type II alpha 1 chain	F 5'-GGATGGCTGCACGAAACAC-3' R 5'-CAGGCGCGAGGTCTTCTG-3'	300
SOX9/Transcription factor SOX9	F 5'-TACCACCTTGTTGCGAATCAGT-3' R 5'-GGTCACACGGTTCTCCATCAT-3'	300
ACAN/Aggrecan	F 5'-GACCACTTTACTCTTGGCGTTTG-3' R 5'-GTCAGGGTCTGAAACGTCTACTGA-3'	500

2.14 Immunofluorescence

Immunofluorescent (IF) reactions were performed on paraffin embedded decellularized cartilage seeded and cultured with chondrocytes to localize collagen type II within the ECM. Briefly, paraffin embedded sections were deparaffinized, rehydrated, and exposed to 10 mM citrate buffer pH 6.0, at a boiling point for antigen retrieval. After cooling, slides were rinsed in a washing buffer and then incubated in blocking buffer (0.3 M glycine, 5% bovine serum albumin in PBS 1X (Sigma-Aldrich, USA)) for 15 min at room temperature (RT). Then, sections were incubated with primary antibody (anti-collagen type II: 2 µg/mL (orb 10436, Byorbit, Cambridge, UK) O/N at 4 °C and with secondary antibody (AffiniPure goat anti-rabbit Alexa Fluor-488 conjugated: 3 µg/ml (111-545-144, Jackson ImmunoResearch, Cambridge, UK) for 45 min at RT. After each step, the sections were washed with PBS.

Lastly, the nuclei were counterstained with 300 nM of DAPI (Cat#D1306, Invitrogen, USA) solution for 5 min and mounted with ProLong Diamond Antifade Mountant (Cat# S36963, Invitrogen, USA). Fluorescent WSI were acquired using a NanoZoomer S60 scanner (Hamamatsu Photonics K.K., Hamamatsu City, Japan).

2.15 Statistical Analysis

The experimental results are reported as means and standard deviation. In all experiments, each treatment was performed in triplicate. Statistical analyses were performed using Prism 8 software (GraphPad Software Inc., San Diego, CA). One and Two-way analysis of variance (ANOVA) were performed, followed by Dunnett's or Tukey's multiple comparisons post hoc tests. For all the applied tests, a $P < 0.05$ (*) was considered as statistically significant.

3 Results

3.1 Decellularized cartilage characterization

Morphological, chemical and ultrastructural investigations were performed on the cartilage disks to verify the decellularization efficacy. The native equine cartilage used as control showed the classical hyaline cartilage morphology with randomly dispersed lacunae characterized by chondrocytes embedded in an extensive ECM (Figure 2A, C). The decellularized cartilage displayed a well-preserved ECM with empty lacunae without any cellular debris, confirming the decellularization effectiveness (Figure 2B). Nuclear counterstaining with DAPI revealed strong fluorescence in cells from native cartilage, while no cells were

observed in the decellularized cartilages (Figure 2C, D). From the ultrastructural standpoint, SEM analysis showed a preserved ECM microarchitecture, featured by a compact fibrillar matrix, and rounded, empty lacunae, providing further evidence that decellularization had properly taken place (Figure 2E, F). Decellularization was also confirmed through the quantitative assessment of DNA content (Figure 2G). In addition, the quantitative analysis of the water absorption ratio (Figure 2H) showed that the decellularization process did not alter this parameter, demonstrating comparable results between the decellularized and the native tissue.

3.2 Cell behavior on the decellularized cartilage

Chondrocytes at P2 showed a greater capacity of adhesion to the disk of dECM compared to P4 cells, in both normoxia and hypoxia conditions. Histological analysis, performed after 2 weeks of culture, showed multiple layers of P2 cells with a roundish morphology, whereas the P4 chondrocytes formed a monolayer characterized by a flattened cell morphology (Figure 3A). The histological observation was supported by the results of cell proliferation assay (Figure 3D), which showed a statistically significant decrease in cell proliferation at P4. The different oxygen conditions did not substantially affect the proliferation; however, hypoxia seemed to stimulate the production of extracellular matrix, resulting in a more abundant and compact matrix as revealed by both Picrosirius red and Toluidine blue stains (Figure 3B, C). This was also supported by collagen quantification (Figure 3E). Electron microscopy analysis revealed that chondrocytes were uniformly distributed and formed a monolayer on the surface of the dECM (Figure 4). At both P2 and P4, cells showed a roundish morphology with a slightly prominent nucleus and formed homogeneous monolayer sheets with a high degree of cell-cell interaction (Figure 4). ECM synthesis appeared particularly evident in P2 cells exposed to hypoxic condition (Figure 4G).

3.3 Gene expression on decellularized cartilage

When used as substrate for chondrocytes, the dECM significantly improved the expression of typical markers of chondrocyte maturity, namely collagen II and aggrecan, related to fibrillar and proteoglycan synthesis (Figure 5A, E). The combination of dECM and hypoxia sustained collagen II expression in both P2 and P4 chondrocytes, whereas P4 cells did not reach the same expression levels under normoxic condition. This result was confirmed via immunofluorescence analysis (Figure 5F), which displayed an increased level of collagen II within the extracellular matrix newly deposited by chondrocytes during hypoxia. Aggrecan expression remained high in all the experimental conditions tested (Figure 5A). Consistent with the data reported above concerning matrix markers, the expression of the chondrogenic transcription factor Sox9 resulted increased by hypoxia in both P2 and P4 chondrocytes (Figure 5B). However, dedifferentiation markers, collagen I and Runx2, were significantly increased only in P4 cells under normoxia and hyperoxia conditions (Figure 5C, D).

3.4 SELP structure

SEM analysis of SELP hydrogels showed a 3D porous microarchitecture featured by a well interconnected structure without morphological differences between the different conditions tested, solvent (dH_2O or PBS) and time (24 h and 72 h) (Figure 6A-D). The analysis of histological sections revealed that chondrocytes cultured onto the SELP maintain the physiological roundish morphology along with the organization in multicellular clusters (Figure 6E, F). The cytocompatibility of the SELP hydrogel was confirmed by MTT analysis, which showed no cytotoxicity during the incubation time, characterized by an initial phase of adaptation up to 4 days, followed by a cell activation phase. After 7 days of incubation, cells started to slightly lose their ability to proliferate compared to plastic (cell culture plates) seeding ($P < 0.05$), indicating a loss of differentiation state on the 2D cultures (Figure 6G). To evaluate structural changes deriving from the solvents and/or incubation time, the secondary structure of SELP was assessed by FTIR (Figure 7). Secondary structure

analysis with curve fitting was performed in the amide I band region (1600 – 1700 cm^{-1}), which originates from the C=O stretching vibration of the amide group and is the most sensitive spectral region used for protein studies (Correia et al., 2019; Fernandes et al., 2018; Pereira et al., 2017). For all samples, more than half of the secondary structures are attributed to β-structures (β-sheets and aggregated strands), which are characterized by strong hydrogen bonding between the polypeptide chains (Machado et al., 2015; Pereira et al., 2017). Comparing the different conditions (solvent and incubation time), no relevant changes were observed in the quantitative structural analysis (Figure 7). Since the hydrogel was proposed as a bioadhesive, its behavior when subjected to physical stress was preliminary evaluated by an adhesion test over time (supplementary Figure S1).

3.5 Rheological test

To better characterize the proposed materials in terms of mechanical features and to assess the behavior of the individual parts of the system under physical stress, the rheological analysis was performed on the SELP, dECM and ECM (Figure 8). The amplitude sweep test showed that from 0 to 1000 Pa of amplitude, the hydrogel and the ECM were still in the linear viscoelastic region (LVER), as both the storage G' and loss G'' moduli remained constant, with higher G'. It is worth noting that some peaks are observed in the G' and G'' plots for both the ECM and dECM, but this is most likely due to the irregular shape of the pieces analyzed, which did not allow a consistent gap of 0.5 mm throughout the whole sample. Consistently with the results of the frequency sweep test, again the G' and G'' remained constant, indicating the expected viscoelastic behavior of the hydrogel and the ECM in the frequencies applied. The test also highlighted a decrease in the complex viscosity |η*| with increasing frequencies, showing a shear-thinning behavior of all the tested materials, effectively leading to a more liquid-like state in higher frequencies. This behavior is further highlighted by the viscosity curve, where the viscosity η decreases linearly as the share rate increases. Finally, the viscosity curve showed higher yield stress and viscosity of the SELP hydrogel in comparison to the native cartilage, which showed lower viscosity, probably because of its structural organization, unlike SELP which, instead, showed values very similar to those of native tissue.

4 Discussion

In this study an ECM stemming from decellularized cartilage of animal origin, specifically from equine metacarpophalangeal and metatarsophalangeal joints, was evaluated in vitro and proposed as structural substitute of articular cartilage to enhance tissue regeneration. The use of dECM has revealed great potential for clinical use and is widely expanding in the fields of tissue engineering and regenerative medicine as a natural alternative for cartilage repair. Decellularized cartilage can be used to produce scaffolds or three-dimensional supports that enable cartilage tissue engineering and can be used to provide a favorable environment for cartilage repair and regeneration by facilitating the adhesion and growth of cartilage tissue progenitor cells (Cheng et al., 2014; Stone et al., 2023). The decellularization approach displays the advantage to preserve natural tissue ECM while simultaneously obliterating the specific cells in tissues or organs allowing to obtain biomimetic scaffolds with promising biological and biomechanical properties (Morris et al., 2017). A proper decellularization process preserves the complex ECM biomolecular and physical cues, thus boosting cell growth and viability (Kim et al., 2019) as confirmed by our results in terms of both cell proliferation and chondrocyte phenotype maintenance, proved by gene expression analysis and newly formed matrix deposition. The use of dECM as a scaffold material is beneficial over the use of other natural and synthetic materials, as it inherently keeps the bioactivity and properties of native tissue. Decellularization is the most effective method to guarantee the biocompatibility of biological derived scaffold, reducing tissue and organ immunogenicity. With regards to decellularization protocols, several methods have been proposed to retain as much of the tissue's bioactivity as possible while maximizing the removal of nuclear material (Xia et al., 2019). To ensure a high quality decellularization process we strictly

followed the guidelines published on this topic (Kasravi et al., 2023). Our results showed an optimal removal of native cartilage cells without altering the biomechanical properties of the tissue. At the same time, no loss of bioactivity of the native cartilage was evident, as the dECM sustained the proliferation of the chondrocytes cultured on decellularized cartilage. Furthermore, the ability to secern extracellular matrix, as particularly shown in the P2 cells, is clear evidence of the maintenance of cartilage bioactivity after the decellularization process. The main limitation for the use of adult differentiated chondrocytes in cell-based therapy and tissue engineering for the repair of articular cartilage is the difficulty of maintaining their state of differentiation during cell expansion (Ravanetti et al., 2022). In the present study we assessed two dedifferentation states of chondrocytes (P2 and P4) onto the dECM as biomatrix in both normoxia and hypoxia culture condition. Our results demonstrated an increased expression of chondrogenic-related genes when chondrocytes were cultured on dECM. For both ACAN and Collagen type II genes, high expression levels show chondrogenic differentiation, except for P4 cells under normoxic conditions, being statistically lower than P2 cells under the same conditions. The latter result probably reflects the reduced ability of late-stage chondrocytes to adapt to a normoxic condition. The chondrogenic transcriptional factor SOX9 also shows high expression under all experimental conditions, except P2-stage chondrocytes in normoxia. These results agree with previous studies demonstrating the positive effect of microenvironmental factors such as hypoxia on the maintenance of chondrocyte differentiation in culture (Ravanetti et al., 2022). Finally, the expression levels of the RUNX2 and Collagen type I genes, which normally are not expressed by cells that are differentiating towards the chondrocytic lineage, confirmed what has been observed. The low levels of RUNX2 and Collagen type I in P2 stage chondrocytes compared to P4 show a greater capacity of the first to differentiate. All together this data clearly indicates that the decellularized biomatrix represents a favorable environment for the maintenance of the chondrogenic phenotype which is also favored by hypoxic conditions.

The mechanical stability at the implantation site is an essential requirement for the use of any biomaterial for regenerative medicine applications. For our cartilage patch we propose a natural hydrogel to make the structure adherent to the subchondral bone. Hydrogels for tissue engineering, derived from various sources of both natural and synthetic origin, have recently attracted huge attention in cartilage regeneration research thanks to the similarity in their features to those of cartilaginous tissue, such as the capacity to absorb large amounts of water while maintaining their structure. In view of the ability to mimic the native tissue, hydrogel development is currently a new frontier in the research addressed to treat cartilage defects (Han et al., 2018; Wang et al., 2014). The biocompatibility and preliminary outcome of the bio-adhesive properties of SELP make it promising to be considered as a biological glue. SELP are designed to combine the high mechanical and tensile strength of silk with the high resilience of the elastin in a single structure (Borrelli et al., 2020; Katari et al., 2015; Machado et al., 2013a). These artificial block copolymers are based on repetitive amino acid sequence motifs commonly found in silk and elastin. SELP are biocompatible and can be processed into different nano- and macrostructures such as hydrogels, fibers, and films (Chang et al., 2011; Huang et al., 2015; Zeng et al., 2014). SELP fiber mats, beside not being cytotoxic, support cell adhesion and proliferation of human skin fibroblast confirming their suitability for tissue engineering applications (Machado et al., 2013b) and have emerged as a promising biomaterial due to their unique properties, including self-assembly, biocompatibility and tunable mechanical properties. Concerning the preparation of SELP in different dissolution media, we have demonstrated that both water and PBS are adequate solvents, and do not exert significant changes at the morphological or structural level. This further supports the versatility of SELP processing as, depending on the application, solvents with different ionic strengths can be used. For instance, water can be employed for various applications, such as surface coating and drug delivery (Huang et al., 2015), while preparation of SELP with PBS provides a pH-balanced environment for specific biological and medical applications requiring buffering capacity. Furthermore, the buffering capacity of PBS can help

maintain a stable pH of the SELP even in the presence of acidic or basic substances (Dandu et al., 2009). This may be particularly important in biomedical applications where gel-like solutions may be exposed to different pH levels. In general, the choice of water or PBS for preparing SELP depends on the intended application, the stability and solubility of the protein, and the pH requirements of the system. In our experiments, the bio and cyto-compatibility of SELP-based materials showed no cytotoxicity, supporting the adhesion and proliferation of chondrocytes at different experimental times. This finding confirms the suitability of using SELPs for tissue engineering applications (Machado et al., 2013b).

The rheological tests highlight several interesting properties about the tested materials. First, it is noticeable that both the hydrogel and the ECM present a viscoelastic behavior, indicating their ability to be subjected to physical stress and strain without suffering structural ruptures, which is of utmost importance when considered for a potential scaffold for osteochondral lesions. Moreover, while it seems that higher shear rates lead to a decrease in viscosity, this should not have an impact on the structural integrity of the gel and could make it more convenient for its application and spreading on the potential lesion site. Lastly, the decellularization process does not lead to any significant difference in the physical characteristics of the ECM, highlighting its effectiveness and suitability for a potential scaffold to treat osteochondral lesions.

Given the common structures of silk protein, from which the SELP derives, the high amount of beta sheets is probably the cause of the viscoelastic behavior of the hydrogel, and its capability to withstand shear stress without losing structural integrity for the tested conditions.

Overall, the hydrogel shows very interesting physical characteristics that could be exploited as a bioadhesive for tissue engineering, since it seems to be able to resist physical stress associated with tissue or bone movement, without losing its structural integrity. Interestingly, its shear-thinning behavior could also be of use when considering that the hydrogel has to be applied and spread over non-homogeneous surface. FTIR spectra indicates that the high percentage of secondary beta structures could be the main cause of these physical properties. A previous study demonstrated that SELP-47 K hydrogel can be used as a scaffold to encapsulate and culture human mesenchymal stem cells in chondrogenic medium, inducing their differentiation toward a chondrogenic phenotype (Haider et al., 2008). Accordingly, in our study SELP supports the maintenance of chondrogenic roundish morphology, favoring the aggregation of cells into clusters. Therefore, the proposed SELP hydrogel could be used with the dual purpose of effectively attaching the dECM to the osteochondral bone, but also to successfully maintain cell phenotype in the tissue after construct implantation.

5 Conclusions

In the present study we proposed and in vitro evaluation of an engineered construct to foster cartilage regeneration. Our tissue is composed of decellularized ECM (dECM) obtained from horse joint cartilage, to support tissue regeneration, coupled with a Silk-Elastin-Like Protein (SELP) hydrogel, acting as a biological glue, to guarantee an adequate adherence to the host tissue. Both dECM and SELP display unique properties allowing the creation of tailor-made microenvironments capable of supporting cell growth and differentiation. Moreover, dECM mimics the natural environment of cartilage, making it an attractive option for repairing damaged or diseased cartilage supporting, especially if combined with hypoxia, the differentiation of chondrocytes, even those at P4 displaying a more dedifferentiated phenotype. SELP, alone or in combination with a dECM, used to create cartilage patch is an interesting tool for tissue engineering and regenerative medicine. Collectively, the results of the rheological tests emphasize several interesting properties about the hydrogel, first of all the viscoelastic behavior, indicating hydrogel ability to be subjected to physical stress and strain without suffering structural alterations, feature of utmost importance considering its potential application as bioadhesive. Moreover, while it seems that higher shear rates lead to a decreased viscosity, this should not impact the structural integrity of the hydrogel, making it suitable for

the treatment of load bearing tissue. Overall, the hydrogel holds very interesting physical characteristics that may be a real asset for its application, particularly due to its resistance to the physical stress generally associated with tissue and bone movement. Intriguingly, the shear-thinning behavior of the hydrogel may also make it suitable to be applied and spread over non-homogeneous surfaces. The proposed hybrid biomaterial, while needing to be further tested in preclinical animal models, seems promising for potential applications in the treatment of cartilage defects and injuries.

Figure Captions

Figure 1 Graphic summary of the biomimetic approach combining decellularized cartilage matrix and Silk-elastin-like-protein (SELP) hydrogel for an articular cartilage patch.

Figure 2. Histology of native (ECM) and Decellularized Cartilage Extracellular Matrix (dECM) stained with H&E (A, B), counterstained with DAPI (C, D) and analyzed with Scanning Electron Microscopy (E, F). A-D scale bar = 50 μm; E–F scale bar = 10 μM. Histograms show the chemical quantification of DNA content (G) and water adsorption capacity (H) of ECM and dECM.

Figure 3. Histological microphotographs of dECM cultured with equine chondrocytes at passages P2 and P4 in normoxic and hypoxic culture conditions, stained with H&E (A), Picro Sirius Red (B) and Toluidine Blue (C). (Scale Bar = 100 μm). Figure D shows cell count of P2 and P4 chondrocytes cultured in adhesion under 20% (normoxia) or 5% oxygen (hypoxia) condition for 2 weeks on dECM. Figure E shows the collagen quantification based on Picrosirius Red staining within the newly deposed ECM. Asterisks indicate significant difference (*P < 0.05, ** P<0.01, *** P<0.001) between normoxia and hypoxia condition at P2 or P4 (n = 5).

Figure 4. Scanning Electron Microscopy of chondrocytes cultured on dECM in normoxic conditions at P2 (A, E) and P4 (B, F) and in hypoxic conditions still at P2 (C, G) and P4 (D, H). Scale bar = 10 μm**.**

Figure 5. Gene expression of ACAN (A), SOX-9 (B), RUNX2 (C), types I (D) and type II (E) collagen, in proliferating P2 and P4 chondrocytes cultured in adhesion under 20% oxygen (normoxia) or 5% oxygen (hypoxia) for 2 weeks (n = 5). The gene expression of control (GADPH) is shown as a dotted line. Asterisks within the bars indicate significant difference referred to control. Asterisks above the lines indicate significant difference between P2 and P4 (*P < 0.05, ** P<0.01, *** P<0.001). Immunofluorescence panel (F) shows collagen type II in P2 and P4 equine chondrocytes cultured on dECM in normoxia or hypoxia condition. Scale bar = 100 μm.

Figure 6 Scanning Electron Microscopy of SELP hydrogel in PBS (A, C) and water (B, D) after 24 hours (scale bar = 100 μm). Histology sections (H&E staining) of chondrocytes cultured on the SELP (E, scale bar 50 μm; F scale bar =100 μm). MTT assay of equine chondrocytes cultured on SELP and plastic used as control, after 24, 48 hours and 4, 7 days of culture (G). Asterisks indicate significant difference between substrates (*P < 0.05).

Figure 7 Amplitude sweep test, frequency sweep tests and viscosity curves for the SELP hydrogel, dECM and ECM. For the amplitude sweep, the frequency f was kept constant at 1 Hz, and for the frequency sweep, the amplitude τ was kept constant at 50 Pa. The G' and G'' moduli are represented in the left Y axis, whereas the tan(δ) and |η*| are represented in the right Y axis for their respective graph. The viscosity η is represented as a function of the shear rate γ. In all cases, the temperature was kept at 37 °C and the gap between the plates was 0.5 mm. All tests were run in duplicate, with both replicas being represented.

Figure 8 Curve-fitted second derivative spectra (solid red line) of SELP-based samples in H_2O and PBS after 24 and 72 h. The bands filled in cyan indicate contributions from β-structures. The Gaussian bands (light gray) were fitted iteratively to the amide I band (black dots) using peak positions determined from the second derivative spectrum (A). The fractional distribution of the major secondary structure components is represented in B.

Supplementary Figure S1: A SELP hydrogel was spread between two circular-shaped cardboards of 1.5 mm in diameter. Different loads (50, 150, 300 and 500 g) were applied up to 7 days. ✓Indicates the maintenance of the adhesiveness for the tested conditions.

6 Bibliography

Armiento, A.R., Alini, M., Stoddart, M.J., 2019. Articular fibrocartilage - Why does hyaline cartilage fail to repair? Adv. Drug Deliv. Rev. 146, 289–305. https://doi.org/10.1016/j.addr.2018.12.015

Bankhead, P., Loughrey, M.B., Fernández, J.A., Dombrowski, Y., McArt, D.G., Dunne, P.D., McQuaid, S., Gray, R.T., Murray, L.J., Coleman, H.G., James, J.A., Salto-Tellez, M., Hamilton, P.W., 2017. QuPath: Open source software for digital pathology image analysis. Sci. Rep. 7. https://doi.org/10.1038/s41598-017-17204-5

Boffa, A., Perucca Orfei, C., Sourugeon, Y., Laver, L., Magalon, J., Sánchez, M., Tischer, T., de Girolamo, L., Filardo, G., 2023. Cell-based therapies have disease-modifying effects on osteoarthritis in animal models. A systematic review by the ESSKA Orthobiologic Initiative. Part 2: bone marrow-derived cell-based injectable therapies. Knee Surgery, Sport. Traumatol. Arthrosc. https://doi.org/10.1007/s00167-023-07320-3

Bonnans, C., Chou, J., Werb, Z., 2014. Remodelling the extracellular matrix in development and disease. Nat. Rev. Mol. Cell Biol. 15, 786–801. https://doi.org/10.1038/nrm3904

Borrelli, M.R., Hu, M.S., Longaker, M.T., Lorenz, H.P., 2020. Tissue Engineering and Regenerative Medicine in Craniofacial Reconstruction and Facial Aesthetics. J. Craniofac. Surg. https://doi.org/10.1097/SCS.0000000000005840

Brown, M., Li, J., Moraes, C., Tabrizian, M., Li-Jessen, N.Y.K., 2022. Decellularized extracellular matrix: New promising and challenging biomaterials for regenerative medicine. Biomaterials 289, 121786. https://doi.org/10.1016/j.biomaterials.2022.121786

Chang, J., Peng, X.-F., Hijji, K., Cappello, J., Ghandehari, H., Solares, S.D., Seog, J., 2011. Nanomechanical Stimulus Accelerates and Directs the Self-Assembly of Silk-Elastin-like Nanofibers. J. Am. Chem. Soc. 133, 1745–1747. https://doi.org/10.1021/ja110191f

Cheng, C.W., Solorio, L.D., Alsberg, E., 2014. Decellularized tissue and cell-derived extracellular matrices as scaffolds for orthopaedic tissue engineering. Biotechnol. Adv. https://doi.org/10.1016/j.biotechadv.2013.12.012

Cipriani, F., Krüger, M., de Torre, I.G., Sierra, L.Q., Rodrigo, M.A., Kock, L., Rodriguez-Cabello, J.C., 2018. Cartilage Regeneration in Preannealed Silk Elastin-Like Co-Recombinamers Injectable Hydrogel Embedded with Mature Chondrocytes in an Ex Vivo Culture Platform. Biomacromolecules 19, 4333–4347. https://doi.org/10.1021/acs.biomac.8b01211

Correia, D.M., Ribeiro, S., da Costa, A., Ribeiro, C., Casal, M., Lanceros-Mendez, S., Machado, R., 2019. Development of bio-hybrid piezoresistive nanocomposites using silk-elastin protein copolymers. Compos. Sci. Technol. 172. https://doi.org/10.1016/j.compscitech.2019.01.017

Dandu, R., Cresce, A. Von, Briber, R., Dowell, P., Cappello, J., Ghandehari, H., 2009. Silk-elastinlike protein polymer hydrogels: Influence of monomer sequence on physicochemical properties. Polymer (Guildf). 50. https://doi.org/10.1016/j.polymer.2008.11.047

De Angelis, E., Cacchioli, A., Ravanetti, F., Bileti, R., Cavalli, V., Martelli, P., Borghetti, P., 2020. Gene expression markers in horse articular chondrocytes: Chondrogenic differentiaton IN VITRO depends on the proliferative potential and ageing. Implication for tissue engineering of cartilage. Res. Vet. Sci. https://doi.org/10.1016/j.rvsc.2019.10.024

Fernandes, M.M., Correia, D.M., da Costa, A., Ribeiro, S., Casal, M., Lanceros-Méndez, S., Machado, R., 2018. Multifunctional magnetically responsive biocomposites based on genetically engineered silk-elastin-like protein. Compos. Part B Eng. 153. https://doi.org/10.1016/j.compositesb.2018.09.019

Haider, M., Cappello, J., Ghandehari, H., Leong, K.W., 2008. In vitro chondrogenesis of mesenchymal stem

cells in recombinant silk-elastinlike hydrogels. Pharm. Res. 25. https://doi.org/10.1007/s11095-007-9282-8

Han, L., Liu, K., Wang, M., Wang, K., Fang, L., Chen, H., Zhou, J., Lu, X., 2018. Mussel-Inspired Adhesive and Conductive Hydrogel with Long-Lasting Moisture and Extreme Temperature Tolerance. Adv. Funct. Mater. 28. https://doi.org/10.1002/adfm.201704195

Huang, W., Rollett, A., Kaplan, D.L., 2015. Silk-elastin-like protein biomaterials for the controlled delivery of therapeutics. Expert Opin. Drug Deliv. https://doi.org/10.1517/17425247.2015.989830

Jiang, S., Tian, G., Yang, Z., Gao, X., Wang, F., Li, J., Tian, Z., Huang, B., Wei, F., Sang, X., Shao, L., Zhou, J., Wang, Z., Liu, S., Sui, X., Guo, Q., Guo, W., Li, X., 2021. Enhancement of acellular cartilage matrix scaffold by Wharton's jelly mesenchymal stem cell-derived exosomes to promote osteochondral regeneration. Bioact. Mater. 6. https://doi.org/10.1016/j.bioactmat.2021.01.031

Karuppal, R., 2017. Current concepts in the articular cartilage repair and regeneration. J. Orthop. 14, A1–A3. https://doi.org/10.1016/j.jor.2017.05.001

Kasravi, M., Ahmadi, A., Babajani, A., Mazloomnejad, R., Hatamnejad, M.R., Shariatzadeh, S., Bahrami, S., Niknejad, H., 2023. Immunogenicity of decellularized extracellular matrix scaffolds: a bottleneck in tissue engineering and regenerative medicine. Biomater. Res. https://doi.org/10.1186/s40824-023-00348-z

Katari, R., Peloso, A., Orlando, G., 2015. Tissue Engineering and Regenerative Medicine: Semantic Considerations for an Evolving Paradigm. Front. Bioeng. Biotechnol. 2. https://doi.org/10.3389/fbioe.2014.00057

Kim, Y.S., Majid, M., Melchiorri, A.J., Mikos, A.G., 2019. Applications of decellularized extracellular matrix in bone and cartilage tissue engineering. Bioeng. Transl. Med. 4. https://doi.org/10.1002/btm2.10110

Li, L., Yu, F., Zheng, L., Wang, R., Yan, W., Wang, Z., Xu, J., Wu, J., Shi, D., Zhu, L., Wang, X., Jiang, Q., 2019. Natural hydrogels for cartilage regeneration: Modification, preparation and application. J. Orthop. Transl. https://doi.org/10.1016/j.jot.2018.09.003

Machado, R., Azevedo-Silva, J., Correia, C., Collins, T., Arias, F.J., Rodríguez-Cabello, J.C., Casal, M., 2013a. High level expression and facile purification of recombinant silk-elastin-like polymers in auto induction shake flask cultures. AMB Express 3, 11. https://doi.org/10.1186/2191-0855-3-11

Machado, R., Da Costa, A., Sencadas, V., Garcia-Arévalo, C., Costa, C.M., Padrão, J., Gomes, A., Lanceros-Méndez, S., Rodríguez-Cabello, J.C., Casal, M., 2013b. Electrospun silk-elastin-like fibre mats for tissue engineering applications. Biomed. Mater. 8. https://doi.org/10.1088/1748-6041/8/6/065009

Machado, R., Da Costa, A., Sencadas, V., Pereira, A.M., Collins, T., Rodríguez-Cabello, J.C., Lanceros-Méndez, S., Casal, M., 2015. Exploring the Properties of Genetically Engineered Silk-Elastin-Like Protein Films. Macromol. Biosci. 15. https://doi.org/10.1002/mabi.201500132

Morris, A.H., Stamer, D.K., Kyriakides, T.R., 2017. The host response to naturally-derived extracellular matrix biomaterials. Semin. Immunol. https://doi.org/10.1016/j.smim.2017.01.002

Ngadimin, K.D., Stokes, A., Gentile, P., Ferreira, A.M., 2021. Biomimetic hydrogels designed for cartilage tissue engineering. Biomater. Sci. https://doi.org/10.1039/d0bm01852j

Nurul, A.A., Azlan, M., Ahmad Mohd Zain, M.R., Sebastian, A.A., Fan, Y.Z., Fauzi, M.B., 2021. Mesenchymal stem cells: Current concepts in the management of inflammation in osteoarthritis. Biomedicines 9. https://doi.org/10.3390/biomedicines9070785

Pereira, A.M., Gomes, D., da Costa, A., Dias, S.C., Casal, M., Machado, R., 2021. Protein-engineered polymers functionalized with antimicrobial peptides for the development of active surfaces. Appl. Sci. 11. https://doi.org/10.3390/app11125352

Pereira, A.M., Machado, R., da Costa, A., Ribeiro, A., Collins, T., Gomes, A.C., Leonor, I.B., Kaplan, D.L., Reis, R.L., Casal, M., 2017. Silk-based biomaterials functionalized with fibronectin type II promotes cell adhesion. Acta Biomater. 47. https://doi.org/10.1016/j.actbio.2016.10.002

Ravanetti, F., Saleri, R., Martelli, P., Andrani, M., Ferrari, L., Cavalli, V., Conti, V., Rossetti, A.P., De Angelis, E., Borghetti, P., 2022. Hypoxia and platelet lysate sustain differentiation of primary horse articular chondrocytes in xeno-free supplementation culture. Res. Vet. Sci. 152, 687–697. https://doi.org/10.1016/j.rvsc.2022.09.031

Sani, E.S., Kheirkhah, A., Rana, D., Sun, Z., Foulsham, W., Sheikhi, A., Khademhosseini, A., Dana, R., Annabi, N., 2019. Sutureless repair of corneal injuries using naturally derived bioadhesive hydrogels. Sci. Adv. 5. https://doi.org/10.1126/sciadv.aav1281

Schmittgen, T.D., Livak, K.J., 2008. Analyzing real-time PCR data by the comparative C(T) methodSchmittgen, T.D., Livak, K.J., 2008. Analyzing real-time PCR data by the comparative C(T) method. Nat. Protoc. 3, 1101–1108.. Nat. Protoc.

Shen, X., Shi, H., Wei, H., Wu, B., Xia, Q., Yeo, J., Huang, W., 2022. Engineering Natural and Recombinant Silks for Sustainable Biodevices. Front. Chem. 10. https://doi.org/10.3389/fchem.2022.881028

Stampoultzis, T., Karami, P., Pioletti, D.P., 2021. Thoughts on cartilage tissue engineering: A 21st century perspective. Curr. Res. Transl. Med. 69, 103299. https://doi.org/10.1016/j.retram.2021.103299

Stone, R.N., Reeck, J.C., Oxford, J.T., 2023. Advances in Cartilage Tissue Engineering Using Bioinks with Decellularized Cartilage and Three-Dimensional Printing. Int. J. Mol. Sci. 24, 5526. https://doi.org/10.3390/ijms24065526

Varanko, A.K., Su, J.C., Chilkoti, A., 2020. Elastin-Like Polypeptides for Biomedical Applications. Annu. Rev. Biomed. Eng. 22, 343–369. https://doi.org/10.1146/annurev-bioeng-092419-061127

Wang, D.A., Varghese, S., Sharma, B., Strehin, I., Fermanian, S., Gorham, J., Fairbrother, D.H., Cascio, B., Elisseeff, J.H., 2007. Multifunctional chondroitin sulphate for cartilage tissue-biomaterial integration. Nat. Mater. 6. https://doi.org/10.1038/nmat1890

Wang, H., Cai, L., Paul, A., Enejder, A., Heilshorn, S.C., 2014. Hybrid elastin-like polypeptide-polyethylene glycol (ELP-PEG) hydrogels with improved transparency and independent control of matrix mechanics and cell ligand density. Biomacromolecules 15. https://doi.org/10.1021/bm500969d

Wei, W., Ma, Y., Yao, X., Zhou, W., Wang, X., Li, C., Lin, J., He, Q., Leptihn, S., Ouyang, H., 2021. Advanced hydrogels for the repair of cartilage defects and regeneration. Bioact. Mater. https://doi.org/10.1016/j.bioactmat.2020.09.030

Xia, C., Mei, S., Gu, C., Zheng, L., Fang, C., Shi, Y., Wu, K., Lu, T., Jin, Y., Lin, X., Chen, P., 2019. Decellularized cartilage as a prospective scaffold for cartilage repair. Mater. Sci. Eng. C. https://doi.org/10.1016/j.msec.2019.04.002

Xie, R., Yao, H., Mao, A.S., Zhu, Y., Qi, D., Jia, Y., Gao, M., Chen, Y., Wang, L., Wang, D.A., Wang, K., Liu, S., Ren, L., Mao, C., 2021. Biomimetic cartilage-lubricating polymers regenerate cartilage in rats with early osteoarthritis. Nat. Biomed. Eng. 5. https://doi.org/10.1038/s41551-021-00785-y

Zeng, L., Jiang, L., Teng, W., Cappello, J., Zohar, Y., Wu, X., 2014. Engineering aqueous fiber assembly into silk-elastin-like protein polymers. Macromol. Rapid Commun. 35, 1273–9. https://doi.org/10.1002/marc.201400058

Zhang, Y.S., Khademhosseini, A., 2017. Advances in engineering hydrogels. Science (80-.). https://doi.org/10.1126/science.aaf3627

Zhou, F., Hong, Y., Zhang, X., Yang, L., Li, J., Jiang, D., Bunpetch, V., Hu, Y., Ouyang, H., Zhang, S., 2018. Tough hydrogel with enhanced tissue integration and in situ forming capability for osteochondral

641 defect repair. Appl. Mater. Today 13. https://doi.org/10.1016/j.apmt.2018.08.005
642